



Understanding the nature of “superhard graphite”

Salah Eddine Boulfelfel¹, Artem R. Oganov^{1,2} & Stefano Leoni³

¹Stony Brook University, Department of Geosciences, NY 11794-2100, USA, ²Department of Geology, Moscow State University, 119899 Moscow, Russia, ³Technische Universität Dresden, Institut für Physikalische Chemie, 01062 Dresden, Germany.

Numerous experiments showed that on cold compression graphite transforms into a new superhard and transparent allotrope. Several structures with different topologies have been proposed for this phase. While experimental data are compatible with most of these models, the only way to solve this puzzle is to find which structure is kinetically easiest to form. Using state-of-the-art molecular-dynamics transition path sampling simulations, we investigate kinetic pathways of the pressure-induced transformation of graphite to various superhard candidate structures. Unlike hitherto applied methods for elucidating nature of superhard graphite, transition path sampling realistically models nucleation events necessary for physically meaningful transformation kinetics. We demonstrate that nucleation mechanism and kinetics lead to *M*-carbon as the final product. *W*-carbon, initially competitor to *M*-carbon, is ruled out by phase growth. *Bct-C₄* structure is not expected to be produced by cold compression due to less probable nucleation and higher barrier of formation.

Computational materials design is a central grand challenge of modern science. Recent progress in the development of theoretical methodologies for structure prediction, especially evolutionary algorithms¹, has led to important discoveries confirmed by subsequent experiments^{2,3}. In addition to thermodynamically stable solid phases, metastable modifications are worth exploring both computationally and experimentally because of their sometimes superior physical properties. However, among the infinite number of all possible metastable phases for each compound, only a handful are synthesizable for kinetic reasons. A metastable phase is synthesizable if it has the highest kinetic likelihood of formation at given conditions.

The recently revived debate^{4–9} on the nature of the metastable product of cold compression of graphite^{10–13} represents a special case of interest. The transformation of graphite to the thermodynamically stable cubic diamond occurs at high pressures and temperatures (> 5 GPa and 1200–2800 K) and in the presence of catalysts. At ambient temperature, however, a new phase is formed above 15–19 GPa^{10–13} and the transition is accompanied by clear changes in the physical properties of carbon^{4,7}.

Experiments have reported an increase in the electrical resistivity^{12,14–18} and optical transmittance^{12,15}. Raman spectra measurements up to 14 GPa indicate that the frequencies of the $E_{2g}^{(1)}$ rigid-layer shear mode at 44 cm^{-1} and the $E_{2g}^{(2)}$ in-plane mode at 1579 cm^{-1} increase sublinearly under pressure with initial pressure coefficients of 4.8 and $4.7\text{ cm}^{-1}/\text{GPa}$, respectively¹⁴. Changes indicating the formation of a new phase have been also observed in the x-ray diffraction pattern^{13,16–18} and in the near *K*-edge spectroscopy¹³. More remarkable is the increase in hardness, as evidenced by the ability of the new phase to indent diamond anvils¹³.

The difficulty to resolve the crystal structure of this mysterious superhard phase, which we call “superhard graphite”, from experiments has stimulated theoretical efforts^{4–7}. Hexagonal and cubic diamond have been ruled out because of the absence of their characteristic Raman bands at 1330 cm^{-1} ¹⁹. Amorphization was dismissed because of the persistence of Bragg peaks^{4,13}.

Theoretically, candidate structures with distinct topologies featuring different patterns, combining odd (5 and 7) and even (4, 6, and 8) rings, have been proposed. A low-enthalpy monoclinic structure called *M*-carbon (space group *C2/m*, *Z*=16) was discovered²⁰ using evolutionary algorithm USPEX and was later identified with “superhard graphite”⁴. All carbon atoms in this structure are four-coordinate and form 5-membered and 7-membered rings when the structure is projected in (010). Later, a body-centered tetragonal structure called *bct-C₄* (space group *I4 mmm*, *Z*=8)^{5,6,21} was proposed as another candidate. The four-coordinate carbon atoms form 4-membered and 8-membered rings on the (001) projection. Shortly afterwards, an orthorhombic candidate structure called *W*-carbon (space group *Pnma*, *Z*=16) was proposed⁷. This structure is very similar to that of *M*-carbon, featuring 5-membered and 7-membered rings when the structure is projected in (010). Very recently, an orthorhombic structure, called *oC16-II* (*Cmmm*, *Z*=16), combining even-membered rings (4, 6, and 8) was

SUBJECT AREAS:

MODELLING AND
THEORY

MATERIALS PHYSICS

ELECTRONIC MATERIALS AND
DEVICES

QUANTUM CHEMISTRY

Received
25 February 2012

Accepted
30 April 2012

Published
28 June 2012

Correspondence and
requests for materials
should be addressed to
S.E.B. (sboulfelfel@
notes.cc.sunysb.edu)

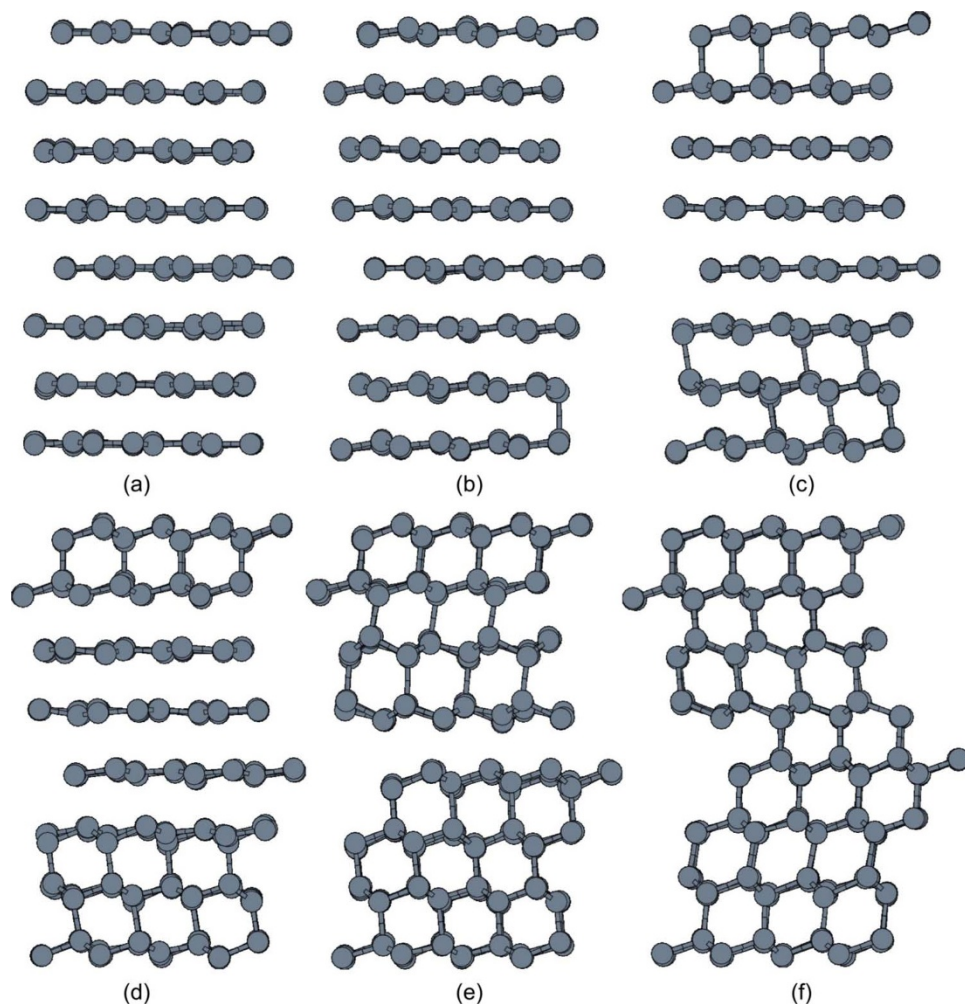


Figure 1 | Snapshots from a dynamical trajectory collected from transition path sampling connecting (a) graphite to (f) a polytype intermediate between cubic and hexagonal diamond. The buckling of graphene layers is initiated by the formation of C–C bonds along $[001]_{\text{graphite}}$ (b)–(c). Domains of cubic diamond are formed with different orientation (d)–(e). The interface between the latter domains defines a region of hexagonal diamond (e)–(f).

predicted using particle-swarm optimization method⁸ and metadynamics simulations⁹. Using the latter method, it was demonstrated that a large variety of superhard structures can be expected (e.g. *oC16-I*, *mC12*, and *mC32*)⁹.

The simulated x-ray diffraction patterns of the predicted structures (*M*-carbon, *W*-carbon, *bct-C₄*, and *oC16-II*) are in satisfactory agreement with experimental data^{4,5,7,9}. Their respective bulk moduli (and hardness²²) are 392.6 (82.7), 391.8 (83.1), 393.4 (82.0), and 408.4 (84.4) GPa⁹. Band gaps calculated using the GW method²³ are 5.00²⁴, 4.39⁷, and 3.78 eV⁵, for *M*-carbon, *W*-carbon, and *bct-C₄*, respectively. All candidate structures show no imaginary phonon frequencies and can explain the experimental observations of hardness and transparency of cold compressed graphite.

Physical properties and energetics of these phases have been theoretically well studied^{4–7,25,26}, but the existing evidence is insufficient to decide which one was obtained in experiments^{10–13}. In order to clearly identify the product of cold compression of graphite, we need to explore graphite transformation kinetics and compute energy barriers for transition regimes characterized by phase coexistence.

Investigations of transition routes to superhard graphite^{6,7} using nudged elastic band method provided inconsistent results, especially inferring that graphite to cubic diamond has lower transition barrier than transformations to other three possible structures⁷. In addition, Ref.⁷ reports a different sequence of energy barriers (cubic diamond < *M*-carbon < *bct-C₄*) from Ref.⁶ (*bct-C₄* < cubic diamond < *M*-carbon), despite the use of the same computational method. These

conflicting results highlight the intrinsic complexity of a reliable elucidation of transition mechanisms and associated barriers.

In a complex system, like a three dimensional solid, the lowest energy state of a system is not always the most relevant²⁷. The viability of any candidate structure as a metastable product is strictly connected to the corresponding transformation pathway and the associated transition barriers or dynamical bottlenecks^{1,28,29}. Transition barriers can be computed and bottlenecks identified with (stationary) saddle points representing transition states on the potential energy surface³⁰. In complex systems with very rugged energy landscapes, saddle points cease to be characteristic points of the free energy barrier³¹. The latter barrier encompasses a large set of configurations and the associated relevant degrees of freedom are very difficult to anticipate^{1,30,31}. To overcome this problem, we can use transition path sampling, a method based on collecting ensembles of dynamical trajectories^{1,28–31}.

Results

In this work, we elucidate the nature of the metastable product of cold compression of graphite and compute the associated energy barrier from true dynamical pathways. The mechanistic details of this pressure-induced phase transformation are determined at the atomic level with full account for relevant events of nucleation. To achieve a reliable and detailed mechanistic picture of the transition we employ a strategy that combines isothermal-isobaric (*NpT*)

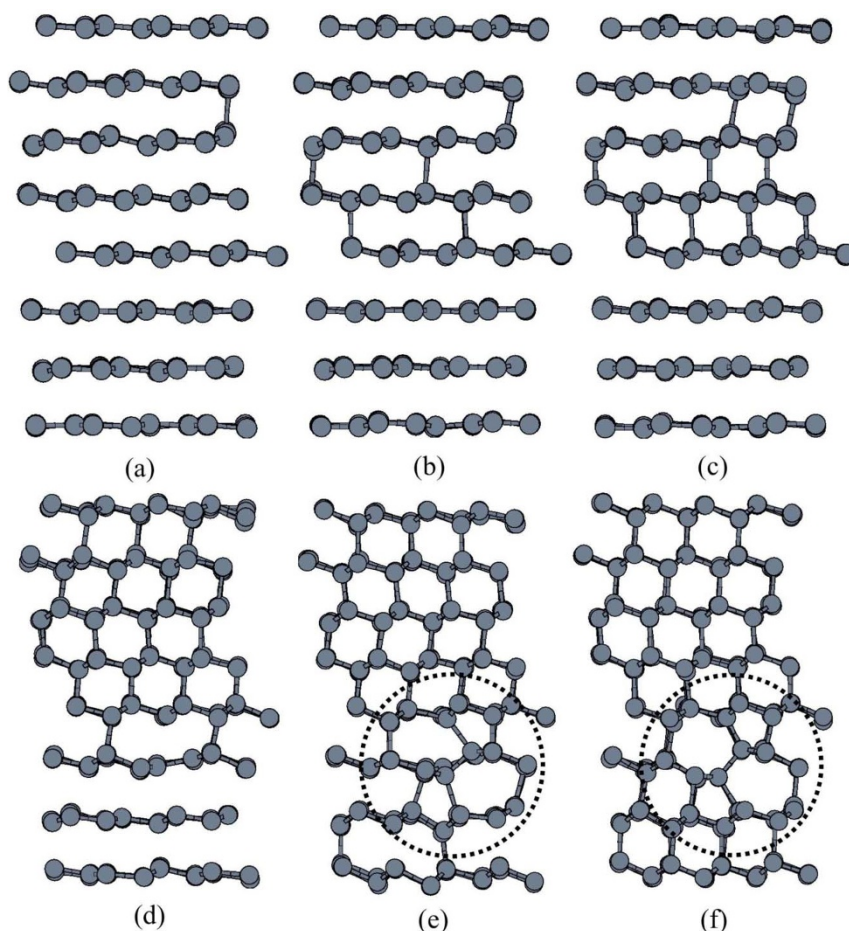


Figure 2 | Snapshots from a representative trajectory illustrating the evolution of the graphite to cubic diamond transition regime. The mobility of graphene layers during the reconstruction creates (d)–(f) an inset of 5- and 7-membered rings (dotted circle) within a 6-membered rings network. This inset interfaces well with cubic diamond and represents the seed of the metastable phase resulting from the cold compression of graphite.

molecular dynamics with transition path sampling (TPS)^{32–34} (see *Methods*). This methodology has proven very effective in the simulation of activated processes^{1,30,35} with phase coexistence and growth^{28,29,36}.

How TPS works. Transition path sampling is a generalization of Monte Carlo procedures in the space of dynamical trajectories connecting two states (graphite and metastable superhard phase in this case) separated by a high barrier in a rough energy landscape^{32–34}. Therein, the relevance of a transition pathway is biased by path probability. The overall simulation approach is iterative and develops from an initial trajectory. By analogy with conventional MC simulations, the first step of TPS consists of equilibrating an initial pathway and gradually converging the trajectory regime to more probable regions. Accordingly, the first trajectory does not need to be a probable one or include mechanistic details of the real transition regime.

In a situation characterized by the possibility of many theoretically viable candidate structures, TPS is a very helpful simulation strategy because it allows starting from a regime of very low probability or even a model constructed from a mapping between the limiting phases of the transition of interest. The convergence is ensured by Monte Carlo sampling of the space of trajectories. In the case of cold compression of graphite, we started from a pathway connecting graphite to cubic diamond generated by propagation of configurations obtained from a modeling approach based on transforming periodic nodal surfaces calculated from a short Fourier summation for each structure^{37,38} (see *Methods*).

Finding the real transition route. The importance of nucleation events during the compression of graphite was pointed out for the transition to diamond at high pressures and temperatures³⁹. In the following, we investigate the kinetics of graphite transformation at ambient temperature due to intrinsic differences between nucleation and growth patterns of predicted superhard structures.

The first set of TPS runs was started from trajectories connecting graphite to cubic diamond. Since diamond (cubic and hexagonal) was ruled out by experiments¹⁹ and due to high activation barrier separating diamond from graphite, starting with this pathway will not only optimize the search in the path ensemble but will help converging to a more probable end point structure. The appearance of a new different phase instead of diamond is allowed by setting a flexible order parameter that can accommodate all four-coordinate structures (see *Methods*).

The set of transition pathways harvested in the course of TPS iterations shows a quick departure of the trajectory regime from the collective motion inherited from the geometrical modeling. The graphite-diamond trajectories underwent three drastic shifts in the transition regime.

First, after 15–20 iterations, the end point of the initial trajectory, graphite to cubic diamond, is replaced by a polytype intermediate between hexagonal and cubic diamond (Fig. 1). The appearance of this polytype is due to opposite sliding directions of graphene layers giving rise to layers of hexagonal diamond. This evolution of the transition regime is similar to the results of a molecular dynamics investigation of the pressure-induced transformation path of graphite of diamond at high temperatures⁴⁰.

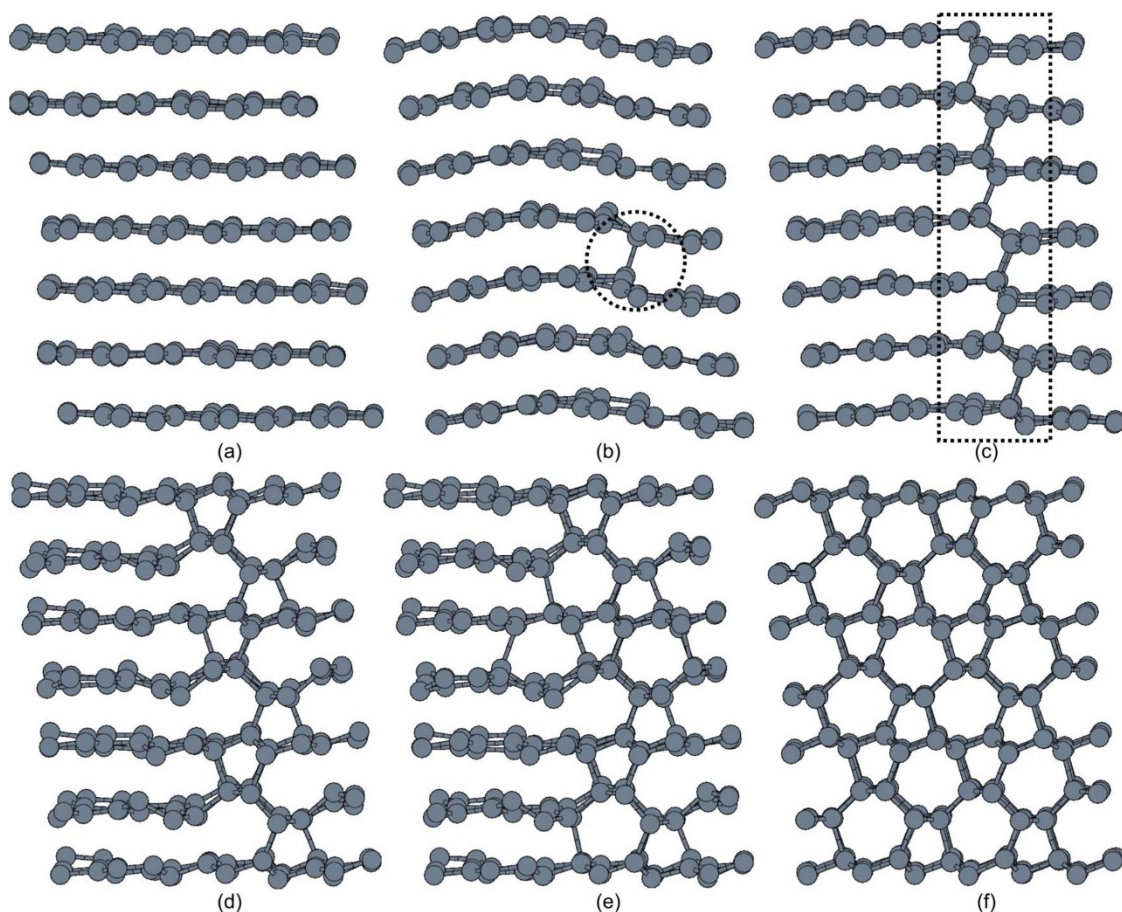


Figure 3 | Snapshots of a representative trajectory of the stable regime corresponding to the cold compression of graphite. A single event of (a) bond formation (dotted circle) between graphene layers triggers (b) a series of bond formation along $[001]_{\text{graphite}}$ in a zigzag fashion (dotted rectangle). The latter contacts facilitate the formation of (c)–(d) 5-membered rings causing the corrugation of graphene layers and inducing the formation of (d)–(e) 7-membered rings.

After 30–40 iterations, an inset of new structural patterns made of 5-membered and 7-membered rings appeared within 6-membered rings network (Fig. 2, (d)–(f)). These new patterns are still made of four-coordinate carbon atoms and interface very well with cubic diamond. They are characteristic of two structures suggested as metastable product for the cold compression of graphite, *M*-carbon and *W*-carbon. The small size of the inset, however, does not yet allow to discriminate between these two models (Fig. 2, (f), dotted circle).

Upon further sampling of the pathway ensemble, the inset of odd-membered rings grew larger and converted the remaining cubic diamond regions into a structure identical to that of *M*-carbon. The new transition regime connects graphite to *M*-carbon (Fig. 3). Therein, the onset of the transformation is marked by the formation of interlayer single C–C bond (Fig. 3, (a)). The formation of the nucleus triggers a series of bond formation events along $[001]_{\text{graphite}}$ in a zigzag fashion (Fig. 3, (b)). The breaking of π -interactions within graphene layers by the emergence of the latter zigzag chain induces layer corrugation that facilitates the formation of 5-membered rings (Fig. 3, (c)–(d)). The latter rings pair up, and additional 7-membered rings are formed (Fig. 3, (e)).

The degrees of freedom induced by the mobility of graphene layers under pressure theoretically allow to consider different ways of graphene layers buckling. The survival of an initial regime or the appearance of a new one is connected to the way of nucleating the high pressure modification and the corresponding free energy barrier. TPS is biased to efficiently converge to the relevant set of the path ensemble which corresponds to the real transition pathway

regime^{29,32–35} and bypasses less-favored regions of the energy landscape corresponding to other mechanisms, graphite-bct- C_4 and graphite-*W*-carbon in this case. To illustrate this feature of TPS, we performed separate simulation runs to evaluate the energy barrier of graphite to bct- C_4 and to *W*-carbon transition routes and clarify the associated reconstruction mechanisms in comparison with the *M*-carbon route.

Viability of graphite to *W*-carbon pathway. Despite its structural and energetic closeness to the *M*-carbon phase⁷, the arrangement of odd-membered rings corresponding to the orthorhombic candidate structure, *W*-carbon, only appears in 20% of trajectories collected during TPS simulations performed starting from graphite to diamond trajectories, over a pressure range from 15–20 GPa.

In order to investigate differences in terms of transition mechanism and kinetics, we modeled a distinct set of TPS runs. The starting trajectory was taken from the previous runs that converged to graphite to *M*-carbon. Although nucleation events triggering the transition along the graphite to *W*-carbon path (Fig. 4, (a)–(b)) are very similar to that of graphite to *M*-carbon (Fig. 3, (a)–(d)), subsequent growth of *W*-carbon slightly differs from that of *M*-carbon. The formation of a C–C bond bridging two graphene layers, in the case of *W*-carbon, induced the appearance of other bonds along $[001]_{\text{graphite}}$ as shown in Fig. 4. Unlike in the transition mechanism to *M*-carbon, the zigzag chain propagates in a segmented fashion (Fig. 4(b)). The key step in the evolution of graphite toward *M*-carbon or *W*-carbon is the evolution of a single nucleation event, formation of an inter-layer C–C bond, either as infinite zigzag

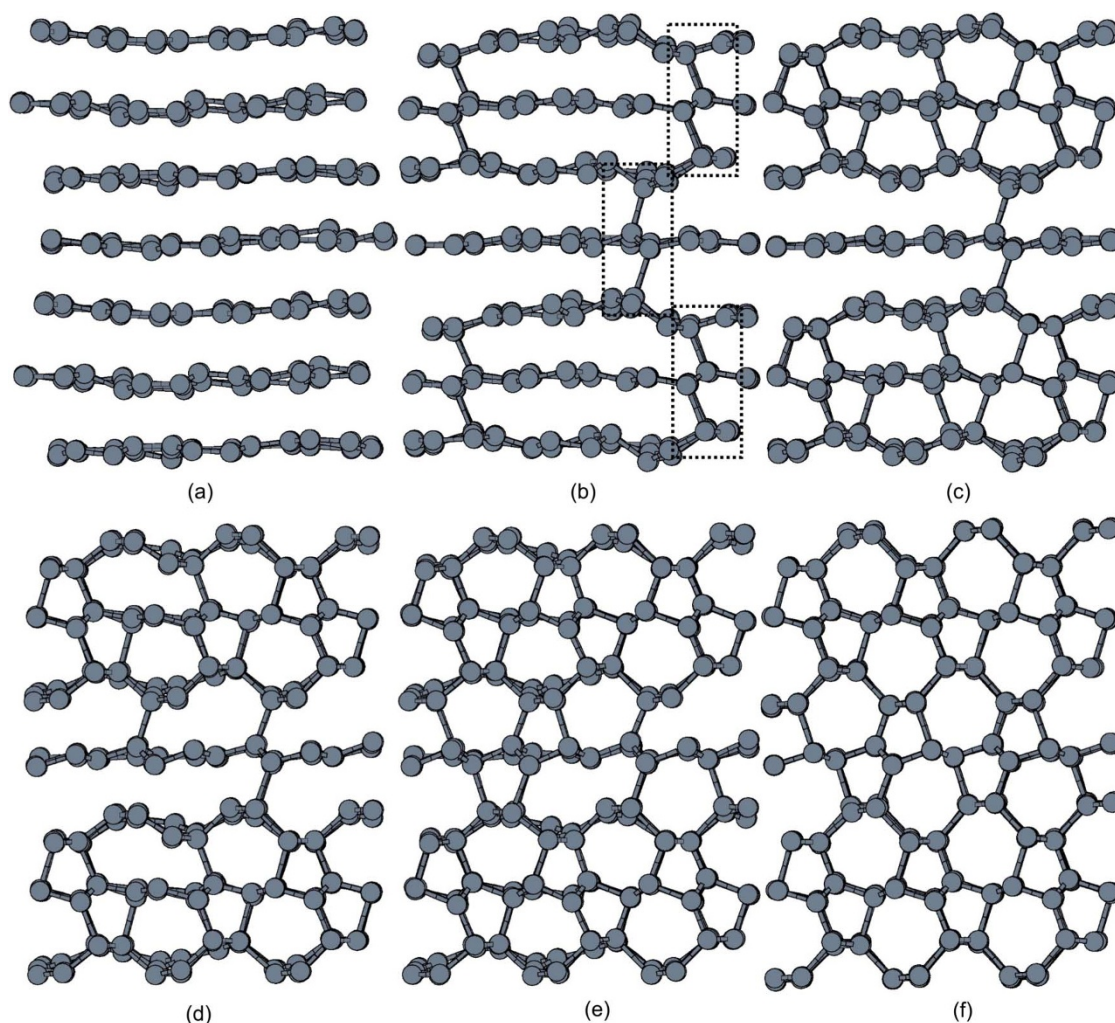


Figure 4 | Snapshots taken from a representative graphite to *W*-carbon transformation pathway. The buckling of graphene layers is initiated by (a)–(b) formation C–C contacts along $[001]_{\text{graphite}}$ in the form of finite size zigzag chains. Each zigzag chain facilitates the corrugation of graphene layers inducing the formation of (c)–(e) 5- and 7-membered rings transforming graphite into (f) *W*-carbon.

(Fig. 3(c)) or segmented chain (Fig. 4(b)). The breaking of the chain implies different progress of phase growth and results in a higher transition barrier (see below for transition kinetics). The average length of graphite to *W*-carbon transformation is 9 ps while graphite to *M*-carbon is 8 ps or less. This reflects slower transition rate for *W*-carbon.

The effect of strain caused by the nucleus on the graphite lattice upon the direct conversion of graphite into diamond has been pointed out to be responsible of the formation of metastable hexagonal modification rather than cubic in agreement with experimental observations³⁹. The nucleus formation along the graphite to *W*-carbon transition induced larger distortions of the graphite structure at the interface if compared to the path to *M*-carbon. This explains the more frequent appearance of the latter structure during the sampling.

Viability of graphite to bct- C_4 pathway. As demonstrated above, the graphite to bct- C_4 path is a less favored route. The set of sampling runs of such a trajectory ensemble quickly shift the transition regime toward the more favorable one, graphite-*M*-carbon. To prevent the disappearance of the bct- C_4 structure, additional constraints are introduced on the order parameter to keep the transition regime as a pure graphite to bct- C_4 transformation (see *Methods*).

A representative trajectory of the latter path is depicted in Fig. 5. Unlike the graphite-*M*-carbon transition mechanism, the onset of

the reconstruction is marked by the formation of two C–C bonds defining a C_4 square unit (Fig. 5, (a)–(b)). The perturbation induced by the C_4 nucleus helps propagating this motif and the bct- C_4 phase grows until complete reconstruction of graphite into the body-centered tetragonal structure.

Kinetics of graphite cold compression. In order to shed light on the kinetics of the transformation of graphite under high-pressure and ambient temperature, enthalpy variation of different simulated transition regimes starting from graphite have been computed and depicted in Fig. 6. The graphite to bct- C_4 transition barrier (Fig. 6, star line) scores as the highest with 221 meV/atom. The graphite to cubic diamond transformation (Fig. 6, circle line) has a barrier of 200 meV/atom which completely rules out the latter transition route for graphite cold compression. Despite the similarities between transformation routes to *W*-carbon (Fig. 6, diamond line) and *M*-carbon (Fig. 6, square line), the latter is favored with a barrier equal to 176 meV/atom, lower than 194 meV/atom for the former transition.

The role of graphene layers sliding. In the nucleation process, the buckling of graphene layers is realized upon their corrugation followed by formation of new C–C bonds (Fig. 1-(b), Fig. 2-(a), Fig. 3-(b), Fig. 4-(a), and Fig. 5-(b)). This is facilitated by layer sliding in graphite that brings carbon atoms into an appropriate stacking sequence for C–C bonds formation along $[001]$. Just prior

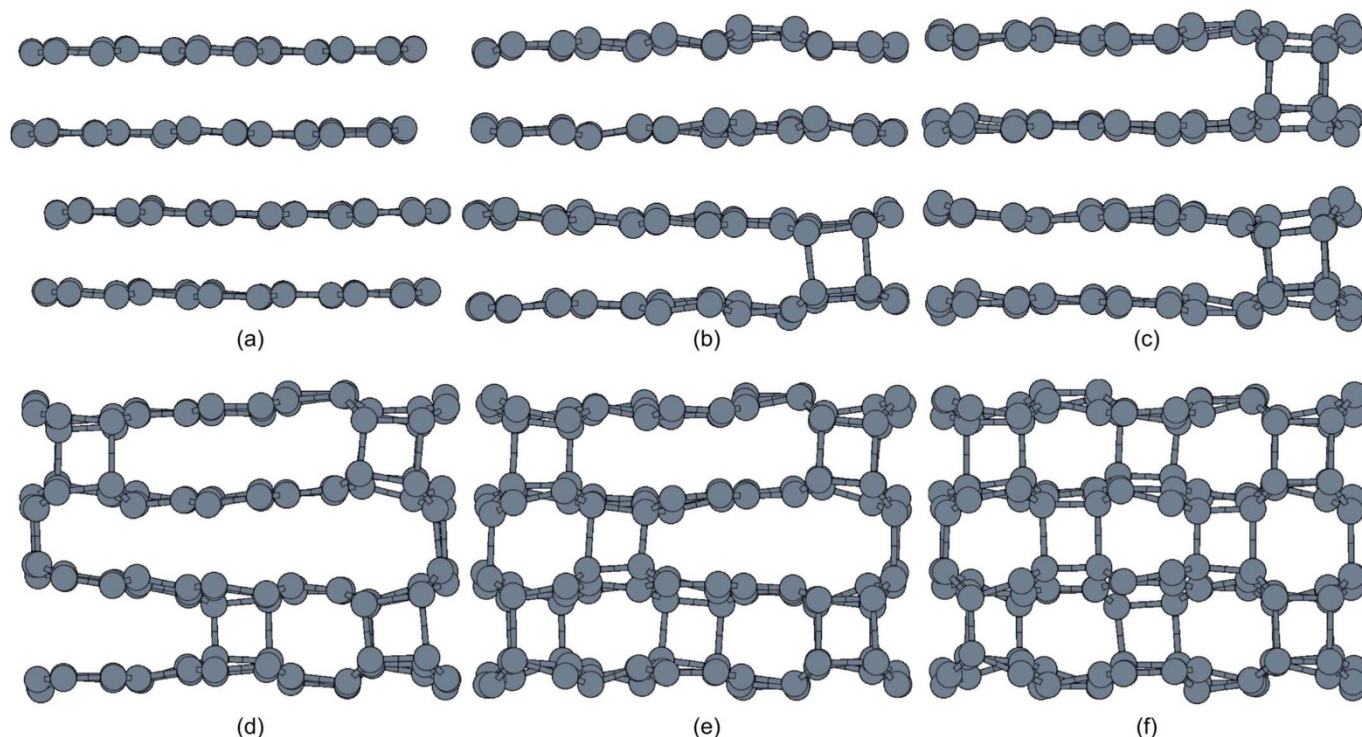


Figure 5 | Snapshots taken from a representative graphite to bct- C_4 transformation pathway. The transition proceeds via nucleation of C_4 square units. Further growth is achieved by corrugation of graphene layers to form more C_4 units and reconstruct the graphite into bct- C_4 .

to nucleus formation, the applied pressure causes graphene layers to slide in a fashion that determines the nature of the high pressure modification to be formed. In Fig. 6, the variation of enthalpy indicates a different evolution for graphite even before the formation of any nucleus for all investigated transformations (graphite to cubic diamond, to bct- C_4 , to W -carbon, and to M -carbon). For $t = 0 - 600$ fs, graphite to bct- C_4 shows a higher enthalpy kink if compared to the two other candidates, W - and M -carbon. This slight

difference in enthalpy (40 meV/atom for bct- C_4 and 30 meV/atom for W - and M -carbon) reflects two different layer sliding mechanisms as shown in Fig. 7. The graphite to bct- C_4 transition requires an eclipsed arrangement of next-neighboring layer along [001] and changes the layers stacking sequence from $\dots AB\dots$ into $\dots AA\dots$ (Fig. 7, (a)–(b)) in order to trigger layers buckling.

The transformations from graphite to 5+7 structures on the contrary require a reduced amount of displacements to induce graphene

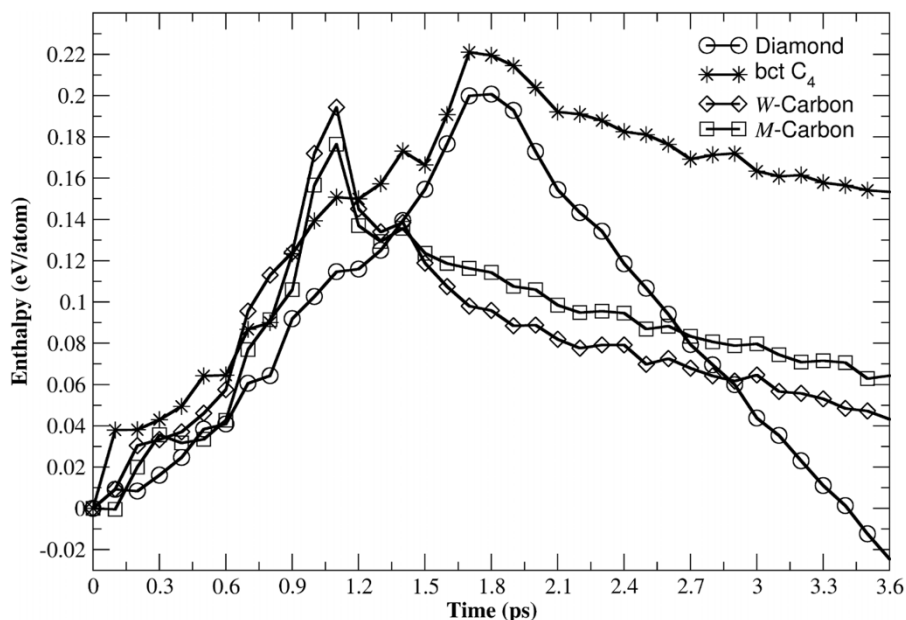


Figure 6 | Enthalpy variation of different simulated transformations of graphite under pressure (15 GPa) and ambient temperature. The graphite to M -carbon transformation route (square line) indicates a lower energy barrier than the transition to W -carbon (diamond line). The possibility of graphite transformation into bct- C_4 structure (star line) on cold compression is ruled out because of higher barrier than the graphite to cubic diamond transition (circle line).

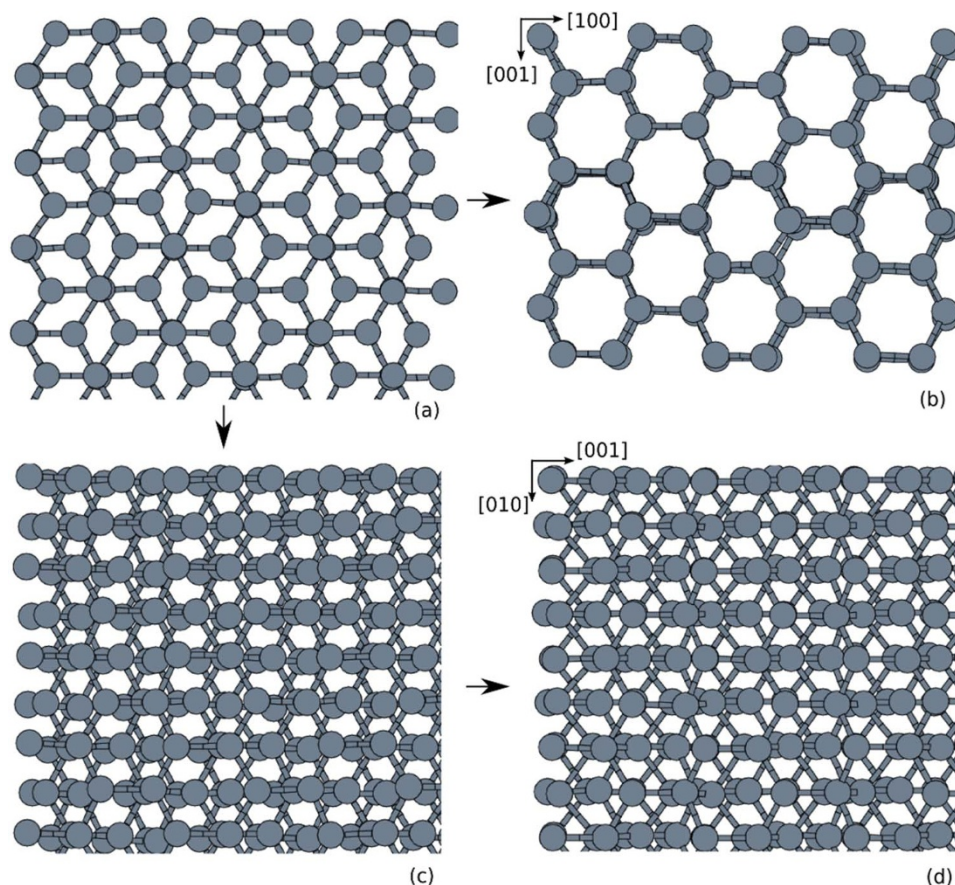


Figure 7 | Top view of graphene layers sliding fashions parallel to (001) plane. The (a) graphite to (b) bct- C_4 transition requires an eclipsed arrangement of next-neighboring layer along [001] and changes the layers stacking sequence from ...AB... into ...AA... in order to trigger layers buckling (only 3 graphitic layers are shown for better clarity). The (a) graphite to (d) *M*-carbon transformation implies small atomic displacements to induce (c) the onset of graphitic layers buckling.

layer buckling (Fig. 7, (a)–(d)). Therefore, transformation routes leading to *W*- and *M*-carbon are more favored than the path to bct- C_4 in terms of layer sliding mechanism in graphite. Additionally, pathways to *W*- and *M*-carbon are less demanding in terms of in-layer distortions, necessary to initiate nucleation.

The stacking sequence and atomic displacements in the case of pathways to *W*- and *M*-carbon imply minimal in-layer distortions in order to initiate nucleation. The path to *M*-carbon is favored over the one to *W*-carbon because of different growth processes making the former structure more probable to form.

The effect of simulation box size has been pointed out in large-scale molecular dynamics simulations of graphite to diamond transition³⁹. If the simulation cell is too small, the derived transition mechanism does not feature in-layer distortions because in-layer stress implies artificial sliding of graphene layers. The size of our simulation box fairly enables the observation of relevant nucleation events and allows to capture distortions around growing nucleus without inducing artificial layer sliding as shown in Fig 3-(c) and Fig 4-(b). Our results underline the role of distortions around the nucleus and how they determine the kinetics and the overall direction of the transformation.

The very recently proposed candidate *o*C16-II deserves special notes. This orthorhombic structure can be described as an alternation of diamond and bct- C_4 slabs along [100] (Fig. 3 in Supplementary Information). The existence of 4-membered rings suggests mechanistic features of buckling in a fashion similar to graphite-bct- C_4 transformation. To reconstruct graphite into a structure with a topology of rings fused as 4 + 6 + 8 pattern, atomic displacements in terms of layers sliding are expected to be larger

than in the mechanism leading to *M*- and *W*-carbon (Fig. 3 in Supplementary Information). On the experimental side, Zhao *et al.*⁸ demonstrated an agreement of the calculated x-ray diffraction pattern of *o*C16-II with the experimental XRD data collected for cold compression of carbon nanotube bundles. The inconsistency with experimental data on “superhard graphite” has been pointed out⁸. In our TPS simulations, the initial graphite to diamond pathway evolved into the graphite to *M*-carbon pathway, bypassing the *o*C16-II structure, in spite of its structural closeness to diamond.

Discussion

Unlike synthesis from the gas phase, the high-pressure synthetic route of superhard graphite depends on the particular nucleation history which would favor one pattern over another at the stage of phase growth within graphite. The viability of transformation routes is not determined by the overall stability of a particular candidate structure, but rather by the activation energy of its formation. Local events of C-C bond breaking and formation control the kinetics of the transition. In this work, an atomistic and kinetic picture of cold compression of graphite is presented using a methodology based on molecular-dynamics simulations combined with transition path sampling. It illustrates how transition path sampling can be used to assess synthesizability of metastable phases by optimizing transformation pathways. Unlike static models, we provide an unbiased description of different dynamical routes and evaluation of the associated transition barriers. The final product of this first-order transformation is unequivocally identified as a metastable monoclinic structure, *M*-carbon. Although a competitor, *W*-carbon is kinetically less favored and differences in transformation rates can be traced



back to different patterns of phase nucleation and subsequent growth. We demonstrate that large distortions caused by the nucleation mechanism of *W*-carbon make it less likely to form than *M*-carbon. Another earlier proposed structures, bct- C_4 , is ruled out because it did not appear during trajectory sampling under cold-compression conditions.

It is worth mentioning that transformation pathways to “superhard graphite” are investigated as homogeneous nucleation processes. The presence of structural defects in the form of interlayer bonds can facilitate nucleation. Consequently, heterogeneous nucleation implies lower activation barriers. However, differences between homogeneous and heterogeneous nucleation do not alter the main features of the transformations revealed in this work. Phase growth kinetics around lattice distortions and structural defects are expected to be similar to that of homogeneous nucleation model. This investigation conducted in this work offers new insights into the understanding of materials synthesizability under high pressure, in a situation of competing phases and in the absence of high-resolution experimental data, and establishes *M*-Carbon as a new carbon allotrope.

Methods

Molecular dynamics simulations. Born-Oppenheimer molecular dynamics simulations were performed in the NpT ensemble³⁰ at temperature $T=300$ K and pressures ranging from 15 to 20 GPa. Constant pressure and temperature were ensured by the Martyna-Tobias-Klein algorithm⁴¹ allowing for anisotropic shape changes of the simulation box. Interatomic forces are computed within the framework of density functional tight binding approach^{42,43} as implemented in the CP2K code⁴⁴. For the accuracy of the set of DFTB parameters⁴⁵ used, see *Supplementary Information*. The time propagation of the system was performed using the velocity Verlet algorithm³⁰. To ensure good time-reversibility an integration timestep of 0.2 fs was used. The simulation box contained 256 carbon atoms. The starting configurations in all simulations correspond to graphite-2H structure. The presence of defects and surface effects on the transition mechanism and the nature of the product of the transition is not investigated because the main focus is set on homogenous nucleation in graphite compressed at ambient temperature.

Transition path sampling. The sampling starts from an initial trajectory connecting the limiting phases. A new trajectory is generated by selecting a configuration from the existing one and slightly modifying the atomic momenta. The modifications δp are applied to randomly chosen pairs of atoms (i, j) according to:

$$\vec{p}_i^{new} = \vec{p}_i^{old} + \delta p (\vec{r}_j - \vec{r}_i) / |(\vec{r}_j - \vec{r}_i)| \quad \text{and} \quad \vec{p}_j^{new} = \vec{p}_j^{old} - \delta p (\vec{r}_j - \vec{r}_i) / |(\vec{r}_j - \vec{r}_i)|,$$

keeping both momentum and angular momentum conserved. The resulting atomic momenta are rescaled by a factor of $\sqrt{E_{kin}^{old} / (\sum_i |\vec{p}_i^{new}|^2 / 2m_i)}$, in order to keep the total

kinetic energy conserved. The propagation of the modified configuration in both directions of time ($-t, +t$) generates a new trajectory. Repeating this step provides a set of trajectories and the successful ones are collected and analyzed. We initialized TPS with trajectories representing four different transformation regimes: graphite-cubic diamond, graphite-bct- C_4 , graphite-*M*-carbon, and graphite-*W*-carbon. Subsequent equilibration of the path ensemble at 300 K and pressures ranging from 15 to 20 GPa in two simulation runs for each transition regime resulted into 8 independent TPS simulation runs. The number of trial shootings for each run exceeded 500 and the acceptance ratio was between 40–60%. This production part of TPS procedure resulted in an ensemble of more than 200 successful pathways, between 8–10 ps long, of which ~ 70 are independent uncorrelated trajectories.

Order parameter. The average coordination number (CN) of carbon atoms is used as an order parameter to distinguish graphite (CN=3) from high pressure modifications made of four-coordinate atoms. All structures discussed in the manuscript (*M*-carbon, *W*-carbon, bct- C_4 , hexagonal and cubic diamond) have an average CN=4 within the first nearest neighbor coordination sphere. In order to narrow down the path ensemble sampling we used second and third nearest neighbors to distinguish between different four-coordinate structures. Clearly, apart from a quick detection of graphite and different candidate structures (bct- C_4 , *M*-carbon, and *W*-carbon), this order parameter is capable of accommodating not only the three possible metastables, like but allows for starting transition pathways sampling from unlikely trajectories, like graphite to cubic or hexagonal diamond. The order parameter does not impose any bias on the evolution of the trajectory sampling.

Topological models. We model transformation paths by transforming periodic nodal surfaces (PNS)^{1,37,38}. The reciprocal space approach implements short Fourier summations to define a family of surfaces according to the formula: $f(x, y, z) = \sum_{h,k,l} |S_{hkl}| |\cos(2\pi(hx + ky + lz) - \alpha_{hkl})|$. S_{hkl} is a geometric structure factor and α_{hkl} is the corresponding phase. The surface corresponding to $f(x, y, z) = 0$ is called PNS. PNS of the transforming phases (A and B) are used as starting points for

the definition of a geometric model for the transition. The choice of a common cell with a constant number of atoms and the periodicity of the model ensure commensurability of the two phases. After transformation of the reflections of the new setting of the cell, the transition can be formulated as a migration from one structure to the other along a coordinate s providing weighted linear mixing of the two functions: $f_{AB}(x, y, z) = s w_A f_A(x, y, z) + (1 - s) w_B f_B(x, y, z)$; $s \in [0, 1]$ To derive the transition state, configurations obtained from the geometric model in the range $s \in [0, 1]$ are propagated in molecular dynamics simulations at 300 K. Random velocities are assigned to atoms and the system is left free to evolve toward either A or B without imposing any bias. Reversing the sign of the time coordinate allows reaching the other phase with a finite probability.

- Oganov, A. R. (ed.) *Modern Methods of Crystal Structure Prediction* (WILEY-VCH, Weinheim, 2010).
- Oganov, A. R. et al. Ionic high-pressure form of elemental boron. *Nature* **457**, 863–867 (2009).
- Ma, Y. et al. Transparent dense sodium. *Nature* **458**, 182–185 (2009).
- Li, Q. et al. Superhard Monoclinic Polymorph of Carbon. *Phys. Rev. Lett.* **102**, 175506–175509 (2009).
- Umamoto, K., Wentzcovitch, R. M., Saito, S. & Miyake, T. Body-Centered Tetragonal C_4 : A Viable sp^3 Carbon Allotrope. *Phys. Rev. Lett.* **104**, 125504–125507 (2010).
- Zhou, X.-F. et al. *Ab initio* study of the formation of transparent carbon under pressure. *Phys. Rev. B* **82**, 134126–134130 (2010).
- Wang, J.-T., Chen, C. & Kawazoe, Y. Low-Temperature Phase Transformation from Graphite to sp^3 Orthorhombic Carbon. *Phys. Rev. Lett.* **106**, 075501–075504 (2011).
- Zhao, Z., Xu, B., Zhou, X.-F., Wang, L.-M., Wen, B., He, J., Liu, Z., Wang, H.-T. & Tian, Y. Novel Superhard Carbon: C-Centered Orthorhombic C_8 . *Phys. Rev. Lett.* **107**, 215502–215506 (2011).
- Selli, D., Baburin, I., Martoňák, R. & Leoni, S. Superhard sp^3 carbon allotropes with odd and even ring topologies. *Phys. Rev. B* **84**, 161411(R)–161415(R) (2011).
- Aust, R. B. & Drickamer, H. G. Carbon: A New Crystalline Phase. *Science* **140**, 817–819 (1963).
- Bundy, F. P. & Kasper, J. S. Hexagonal Diamond - A New Form of Carbon. *J. Chem. Phys.* **46**, 3437–3446 (1967).
- Utsumi, W. & Yagi, T. Light-transparent phase formed by room-temperature compression of graphite. *Science* **252**, 1542–1544 (1991).
- Mao, W. L. et al. Bonding Changes in Compressed Superhard Graphite. *Science* **302**, 425–427 (2003).
- Hanfland, M., Beister, H. & Syassen, K. Graphite under pressure: Equation of state and first-order Raman modes. *Phys. Rev. B* **39**, 12598–12603 (1989).
- Hanfland, M., Syassen, K. & Sonnenschein, R. Optical reflectivity of graphite under pressure. *Phys. Rev. B* **40**, 1951–1954 (1989).
- Zhao, Y. X. & Spain, I. L. X-ray diffraction data for graphite to 20 GPa. *Phys. Rev. B* **40**, 993–997 (1989).
- Takano, K. J., Harashima, H. & Wakatsuki, M. New High-Pressure Phases of Carbon. *Jpn. J. Appl. Phys.* **30**, L860–L863 (1991).
- Yagi, T., Utsumi, W., Yamakata, M.-A., Kikegawa, T. & Shimomura, O. High-pressure *in situ* x-ray-diffraction study of the phase transformation from graphite to hexagonal diamond at room temperature. *Phys. Rev. B* **41**, 6031–6039 (1992).
- Xu, J.-A., Mao, H.-K. & Hemley, R. J. The gem anvil cell: high-pressure behaviour of diamond and related materials. *J. Phys. Condens. Matter* **14**, 11549–11552 (2002).
- Oganov, A. R. & Glass, C. W. Crystal structure prediction using *ab initio* evolutionary techniques: Principles and applications. *J. Chem. Phys.* **124**, 244704–244719 (2006).
- Baughman, R. H., Liu, A. Y., Cui, C. & Schields, P. J. A carbon phase that graphitizes at room temperature. *Synth. Met.* **86**, 2371–2374 (1997).
- Lyakhov, A. O. & Oganov, A. R. Evolutionary search for superhard materials applied to forms of carbon and TiO_2 . *Phys. Rev. B* **84**, 092103–092106 (2011).
- Aryasetiawan, F. & Gunnarsson, O. The GW method. *Rep. Prog. Phys.* **61**, 237–312 (1998).
- Zhu, Q., Oganov, A. R., Salvadó, M. A., Pertierra, P. & Lyakhov, A. O. Denser than diamond: *Ab initio* search for superdense carbon allotropes. *Phys. Rev. B* **83**, 193410–193413 (2011).
- Liang, Y., Zhang, W. & Chen, L. Phase stabilities and mechanical properties of two new carbon crystals. *Europhys. Lett.* **87**, 56003–56008 (2009).
- Wei, P. Y., Sun, Y., Chen, X.-Q., Li, D. Z. & Li, Y. Y. Anisotropy in electronic, optical, and mechanical properties of superhard body-centered tetragonal C_4 phase of carbon. *App. Phys. Lett.* **97**, 061910–061912 (2010).
- O’Keeffe, M. Aspects of crystal structure prediction: some successes and some difficulties. *Phys. Chem. Chem. Phys.* **12**, 8580–8583 (2010).
- Boulfel, S. E., Zahn, D., Grin, Yu & Leoni, S. Walking the Path from B4- to B1-Type Structures in GaN. *Phys. Rev. Lett.* **99**, 125505–125508 (2007).
- Boulfel, S. E., Seifert, G. Grin, Yu & Leoni, S. Squeezing lone pairs: The A17 to A7 pressure-induced phase transition in black phosphorus. *Phys. Rev. B* **85**, 014110–014115 (2012).
- Frenkel, D. & Smit, B. *Understanding Molecular Simulations from algorithms to applications, Second Edition*, (Academic, San Diego), 2nd Ed. (2002).



31. Dellago, C., Bolhuis, P. G. & Geissler, P. L. *Transition Path Sampling Methods*, in Ferrario, M., Ciccotti, G. & Binder, K. (eds), *Computer Simulations in Condensed Matter: From Materials to Chemical Biology Vol 1*, Springer-Verlag, 349–392 (2006).
32. Bolhuis, P. G., Dellago, C. & Chandler, D. Sampling ensembles of deterministic transition pathways. *Faraday Discuss.* **110**, 421–436 (1998).
33. Dellago, C., Bolhuis, P. G., Csajka, F. S. & Chandler, D. Transition path sampling and the calculation of rate constants. *J. Chem. Phys.* **108**, 1964–1978 (1998).
34. Bolhuis, P. G., Chandler, D., Dellago, C. & Geissler, P. L. Transition path sampling: Throwing ropes over rough mountain passes, in the dark. *Annu. Rev. Phys. Chem.* **53**, 291–318 (2002).
35. Zahn, D. & Leoni, S. Nucleation and Growth in Pressure-Induced Phase Transitions from Molecular Dynamics Simulations: Mechanism of the Reconstructive Transformation of NaCl to the CsCl-Type Structure. *Phys. Rev. Lett.* **92**, 250201–250204 (2004).
36. Boulfelfel, S. E. & Leoni, S. Competing intermediates in the pressure-induced wurtzite to rocksalt phase transition in ZnO. *Phys. Rev. B* **78**, 125204–125210 (2008).
37. Leoni, S. & Zahn, D. Putting the squeeze on NaCl: modeling and simulation of the pressure driven B1–B2 phase transition. *Z. Kristallogr.* **219**, 339–344 (2004).
38. von Schnering, H. G. & Nesper, R. Nodal surfaces of Fourier series: Fundamental invariants of structured matter. *Z. Phys. B* **83**, 407–412 (1991).
39. Khaliullin, R. Z., Eshet, H., Kühne, T. D., Behler, J. & Parrinello, M. Nucleation mechanism for the direct graphite-todiamond phase transition. *Nat. Mat.* **10**, 693–697 (2011).
40. Scandolo, S., Bernasconi, M., Chiarotti, G. L., Focher, P. & Tosatti, E. Pressure-Induced Transformation Path of Graphite to Diamond. *Phys. Rev. Lett.* **74**, 4015–4018 (1995).
41. Martyna, G. J., Tobias, D. J. & Klein, M. L. Constant pressure molecular dynamics algorithms. *J. Chem. Phys.* **101**, 4177–4190 (1994).
42. Seifert, G., Porezag, D. & Frauenheim, Th. Calculations of molecules, clusters, and solids with a simplified LCAO-DFT/LDA scheme. *Int. J. Quant. Chem.* **58**, 185–192 (1996).
43. Zhechkov, L., Heine, T., Patchkovskii, S., Seifert, G. & Duarte, H. A. An Efficient *a Posteriori* Treatment for Dispersion Interaction in Density-Functional-Based Tight Binding. *J. Chem. Theo. Comp.* **1**, 841–847 (2005).
44. <http://cp2k.berlios.de> (2011).
45. Porezag, D., Frauenheim, Th., Köhler, Th., Seifert, G. & Kaschner, R. Construction of tight-binding-like potentials on the basis of density-functional theory: Application to carbon. *Phys. Rev. B* **51**, 12947–12957 (1995).

Acknowledgments

This work is funded by DARPA (grant N66001-10-1-4037) and NSF (grant EAR-1114313). S.L. acknowledges support from DFG for support (SPP 1415). Calculations were performed at computing facilities of ZIH (TU-Dresden), CFN at Brookhaven National Laboratory (supported by the U.S. Department of Energy, Office of Basic Energy Sciences, under contract No. DE-AC02-98CH10086), Joint Supercomputer Center of the Russian Academy of Sciences, and Skif-MSU Supercomputer (Moscow State University).

Author contributions

S.E.B., A.R.O., and S.L. designed research, performed simulations, analyzed data, and wrote the manuscript.

Additional information

Supplementary information accompanies this paper at <http://www.nature.com/scientificreports>

Competing financial interests: The authors declare no competing financial interests.

License: This work is licensed under a Creative Commons Attribution-NonCommercial-ShareAlike 3.0 Unported License. To view a copy of this license, visit <http://creativecommons.org/licenses/by-nc-sa/3.0/>

How to cite this article: Boulfelfel, S.E., Oganov, A.R. & Leoni, S. Understanding the nature of “superhard graphite”. *Sci. Rep.* **2**, 471; DOI:10.1038/srep00471 (2012).